


Communication

# Fine Structure of High-Energy Pulses from a Stimulated Brillouin Scattering-Assisted Q-Switch Tm-Doped Fiber Laser

Vladimir A. Kamynin <sup>1</sup>, Serafima A. Filatova <sup>1,\*</sup> , Timur I. Mullanurov <sup>2</sup>, Maksim D. Cheban <sup>1</sup>, Alexey A. Wolf <sup>3</sup> , Dmitry A. Korobko <sup>4</sup> , Andrei A. Fotiadi <sup>5,6</sup>  and Vladimir B. Tsvetkov <sup>1</sup>

<sup>1</sup> Prokhorov General Physics Institute of the Russian Academy of Sciences, 38 Vavilov St., 119991 Moscow, Russia; kamynin@kapella.gpi.ru (V.A.K.); tsvetkov@lsk.gpi.ru (V.B.T.)

<sup>2</sup> Higher Engineering School, National Research Nuclear University MEPhI, 31 Kashirskoe Shosse, 115409 Moscow, Russia

<sup>3</sup> Institute of Automation and Electrometry (IA&E) of the SB RAS, 1 Acad. Koptyug Ave., 630090 Novosibirsk, Russia

<sup>4</sup> S.P. Kapitsa Scientific Technological Research Institute, Ulyanovsk State University, 42 Leo Tolstoy Str., 432970 Ulyanovsk, Russia; korobkotam@rambler.ru

<sup>5</sup> Electromagnetism and Telecommunication Department, University of Mons, B-7000 Mons, Belgium

<sup>6</sup> Optoelectronics and Measurement Techniques Unit, University of Oulu, 90570 Oulu, Finland

\* Correspondence: filatova@kapella.gpi.ru

**Abstract:** We have demonstrated a simple all-fiber thulium (Tm) laser Q-switched by stimulated Brillouin scattering (SBS). The maximum output pulse energy was 80  $\mu$ J. This allowed us to generate a broadband spectrum directly at the laser outputs. For the first time, we measured the fine structure of the output pulses with a resolution of less than 100 ps. It was found that the SBS Q-switched laser is capable of generating bunches of picosecond pulses. The effect of modulation instability on the pulse decay is discussed. The potential application of the investigated laser radiation for producing destructive effects on soft biological tissues has been demonstrated.

**Keywords:** thulium; thulium fiber laser; Q-switch; stimulated Brillouin scattering; bunches of pulses; broadband radiation



**Citation:** Kamynin, V.A.; Filatova, S.A.; Mullanurov, T.I.; Cheban, M.D.; Wolf, A.A.; Korobko, D.A.; Fotiadi, A.A.; Tsvetkov, V.B. Fine Structure of High-Energy Pulses from a Stimulated Brillouin Scattering-Assisted Q-Switch Tm-Doped Fiber Laser. *Photonics* **2024**, *11*, 30. <https://doi.org/10.3390/photonics11010030>

Received: 4 December 2023

Revised: 22 December 2023

Accepted: 27 December 2023

Published: 29 December 2023



**Copyright:** © 2023 by the authors. Licensee MDPI, Basel, Switzerland. This article is an open access article distributed under the terms and conditions of the Creative Commons Attribution (CC BY) license (<https://creativecommons.org/licenses/by/4.0/>).

## 1. Introduction

In recent decades, there has been an interest in laser sources that generate radiation in the 2  $\mu$ m spectral range. Great progress has been made in the field of solid-state lasers based on Tm-YAG and Ho-YAG crystals doped with thulium and holmium ions, respectively [1,2]. These high-power, high-energy lasers are actively marketed and commercially available. However, due to advances in laser technology, fiber lasers have several advantages over solid-state lasers. These include compact all-fiber and robust design, high beam quality, and the ability to achieve different operating modes in a wide range of wavelengths [3].

All-fiber lasers of the 2  $\mu$ m spectral range are in great demand for medical applications [4–6], polymer material processing [7], advanced data transmission systems [8,9], and atmospheric sensing systems [10,11]. Pulsed lasers operating in the 1.9–2  $\mu$ m spectral range can also be used as pump sources for Cr<sup>2+</sup>:ZnSe active elements. [12]. The existence of a wide application range has led to a variety of laser system configurations. They are mostly based on the principle of a master oscillator and amplifier system, where the pulses are shaped by active modulation [13–15]. This, on the one hand, allows flexible control of the output radiation characteristics (duration, peak power, and energy), but on the other hand, increases the complexity of the setup and introduces restrictions on the minimum pulse duration value. Thus, the development of simple pulsed laser systems with passive modulation, emitting in the 2  $\mu$ m spectral range, is an actual task. One of the most promising rare earth elements for active media doping in this spectral region is thulium (Tm<sup>3+</sup>).

Typically, a pulse operation regime can be achieved in a few ways—mode-locking, Q-switching, and gain-switching. In the first mode, pulses from several hundred femtoseconds [16] to nanoseconds [17] have been demonstrated. To achieve this generation mode, one must use saturable absorbers [18], artificial modulators [17], or active modulators [19]. In the case of Tm-doped fibers, some scientific groups have successfully demonstrated the self-pulsing (SP) phenomenon (due to active-ion quenching) [20–22]. These schemes are quite simple and robust. However, in the case of mode-locking, the pulse repetition rate, pulse duration, and energy are fixed as usual. To change the listed parameters, some additional elements (pulse peakers, amplifiers) should be placed into the laser system.

Gain-switching is another attractive way to achieve pulse on demand. In this case, pulses from tens of nanoseconds to microseconds have been demonstrated at the laser output. These lasers have a simple scheme. Usually it consists of an active medium and a pair of mirrors. The key element of this system is a pulsed pump source. Modern laser diode drivers allow high currents (of several amperes) with nanosecond rise and fall times to be achieved. As a result, in [23], the authors demonstrated pulse widths as short as 10 ns. More than 1 kW of peak power was obtained from the gain-switched TDFL, with a fiber core size of 6.3  $\mu\text{m}$ . The authors showed that changing the cavity length from 4.3 to 0.2 m resulted in a reduction in output pulses from 130 to 10 ns. Overall, to create this type of pulsed laser, one needs an expensive pump driver (in the case of a laser diode source) or a modulated pump laser with a power amplifier [24].

The most widely used method for generating high-energy pulses directly from the laser output is Q-switching. One branch of this method is active modulation of the cavity Q factor. The researchers use acousto-optic modulators [14,25] or Pockels cells [26] for this purpose. For example, in [25], the authors experimentally demonstrated the use of the high-speed optical modulator. As a result, stable Q-switched pulses with the ability to tune the pulse repetition rate have been demonstrated. The minimum pulse width has been measured to be  $\sim 160$  ns at 100 kHz. In another work [26], Coluccelli et al. showed the Tm:BaY<sub>2</sub>F<sub>8</sub> laser with output pulses of 170 ns duration at a minimum repetition rate of 5 Hz with an energy of 3.2 mJ. However, active Q-switching also requires complicated optical elements and control electronics.

Therefore, the simplest way to achieve high-energy laser pulses is passive Q-switching. To date, passive Q-switching has been implemented in most fiber lasers using various saturable absorbers, ranging from thin films to fiber absorbers [27–29]. This enables pulse durations from tens of nanoseconds to several microseconds. The energy of pulses ranges from 1 to 50  $\mu\text{J}$ . Pulse repetition rates are controlled by the optical pump power. Obviously, the major disadvantage of these systems is the sensitivity of real absorbers to radiation damage. This can lead to both system failure and gradual degradation of parameters due to increasing unsaturated optical losses in the cavity. One solution is to reduce the number of elements that could be damaged by laser radiation and utilize the nonlinear properties of optical fibers. Therefore, the stimulated Brillouin scattering (SBS) effect is used to realize passive Q-switching in fiber lasers [30–32]. In these works, a ring interferometer is added to the fiber laser scheme to achieve regular and stable pulsed operation. In [33], the authors used a Fabry–Perot interferometer in their laser scheme. This operation principle utilizes cascaded Rayleigh scattering and SBS, which provide dynamic feedback in the fiber cavity [31]. In [34], the authors proposed to achieve distributed SBS feedback in a piece of ultrahigh-numerical-aperture fiber without any interferometers. Pulses with durations of more than 10 ns and energies of up to 50  $\mu\text{J}$  have been obtained in the aforementioned works. However, studies of the fine structure of pulsed radiation at the output of such laser systems have not been presented previously. Additionally, the presented laser configurations can obtain broadband radiation both at the output of the laser [30] and by using dispersion-shifted fibers outside the laser cavity [35].

In this work, we present an all-fiber scheme of a thulium (Tm<sup>3+</sup>) laser operating in the passive Q-switching mode based on the SBS effect, and demonstrate for the first time the generation of sub-nanosecond pulse bunches. The effect of modulation instability on pulse

decay is discussed. Another unique feature is an ultra-broadband spectrum (over 400 nm) generated directly at the laser outputs without the use of additional high nonlinearity index fibers. At the same time, the laser scheme is implemented using only standard optical components. The potential application of the investigated laser radiation with destructive effects on soft biological tissues is demonstrated.

## 2. Experimental Setup

Figure 1 shows the optical scheme of a Tm-doped fiber laser. The active fiber was pumped by a multimode laser diode (LD) through a pump–signal combiner (COMB). The central emission wavelength of the laser diode was 793 nm, and the maximum output power was up to 10 W. A 5 m long double-clad silica-based fiber segment doped with thulium ions (TmDF) with core-clad diameters of 10 and 127  $\mu\text{m}$ , respectively, was used as an active laser medium. The absorption in the clad at a wavelength of 790 nm was  $4.6 \pm 0.5$  dB/m. In the laser cavity, we used a highly reflective fiber Bragg grating (HR FBG) inscribed by femtosecond laser pulses [36]. The reflection peak corresponded to a wavelength of 1960 nm, and the reflection coefficient was  $R = 96\%$ . Similar to the work [31], a ring interferometer was placed in another part of the cavity, opposite the HR FBG. The interferometer was based on the X-type 90/10 coupler, and 10% of the output was connected to the free input via an 8 m standard single-mode delay fiber (SMF). Fiber optic connectors with 8-degree angle polishing (FC/APC) were used for output and control of laser radiation at outputs 1 and 2.

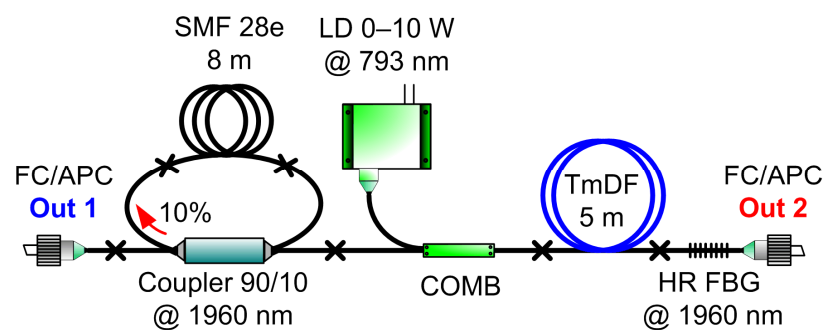


**Figure 1.** Optical scheme of a Tm-doped fiber laser. COMB—pump–signal combiner, LD—laser diode, TmDF—thulium-doped fiber, HR FBG—highly reflective fiber Bragg grating, SMF—single-mode fiber.

We measured temporal, spectral, and energy parameters of laser radiation from both laser outputs during the experiments. Spectral measurements were performed with a 0.1 nm resolution optical spectrum analyzer (OSA). The temporal parameters of the pulse radiation were analyzed using an oscilloscope and a photodetector with a maximum temporal resolution of 0.1 ns. A pyroelectric energy meter operating in the range of 1  $\mu\text{J}$  to 10 mJ in the spectral range of 0.15–12  $\mu\text{m}$  was used to measure the pulse energy.

## 3. Experimental Results and Discussion

The physical processes behind Brillouin Q-switching can be explained in terms of open cavity modes, taking into account some fundamental nonlinear properties of standard silica-based fibers. The use of high-quality fiber in the laser cavity ensures a fairly uniform distribution of refractive index irregularities (i.e., “frozen” Rayleigh reflectors) along the entire fiber, which acts as a distributed Rayleigh mirror. Using Tm-doped fiber as the active medium for light amplification provides lasing, which allows gain heterogeneity due to spectral hole-burning. The appearance of the laser resonance properties can be considered the result of a nonlinear selection of the most successful open cavity modes. Physically, this means that among the photons with complex “paths” trapped in the cavity, some will return to their initial states more often than others. Therefore, when Tm-doped fiber amplification begins to compensate for fiber loss, these resonant photons reach lasing

conditions first. This results in the generation of narrowband components in the laser spectrum [37].

In turn, the generation of narrowband spectral components in the pumped laser cavity leads to avalanche-like Brillouin instabilities, which often appear as multiple spikes in the spectral and temporal domain. Brillouin scattering due to interaction with acoustic phonons provides narrowband Stokes-shifted optical gain. For a monochromatic pump at 1960 nm, the Brillouin gain factor is nearly three orders of magnitude higher than the Raman gain, providing amplification with a bandwidth of ~20 MHz at a frequency downshift of ~8.7 GHz from the pump frequency. Occasional lasing of a narrowband spectral component due to residual cavity resonance induces additional Brillouin gain for downshifted modes, leading to their rapid (exponential) growth [38]. This cascading process transfers power from high-frequency components to lower-frequency components, providing a higher growth rate (and higher peak power) for the new frequency components. This continues until the generation of short pulses by the latest cascades exhausts the accumulated cavity power. The described pattern is typical for all fiber lasers employing distributed Rayleigh feedback [30,37,39]. A more detailed theory of the passive Q-switching mode based on the SBS effect supported by equations has been presented previously, e.g., in [31].

The radiation characteristics were measured from both the interferometer side and the HR FBG side. We observed several modes of operation during the research: continuous-wave, transient, and pulsed. A continuous-wave operation mode was observed after exceeding the generation threshold at a pump power of 2.5 W and up to 2.9 W of pump power. At the same time, a narrowband spectrum corresponding to the resonance reflection peak of the FBG at a wavelength of 1960 nm was measured at output 1 (Figure 2a). The contrast with respect to the amplified spontaneous emission exceeded 20 dB. The average power detected at output 1 in this mode did not exceed 100 mW.

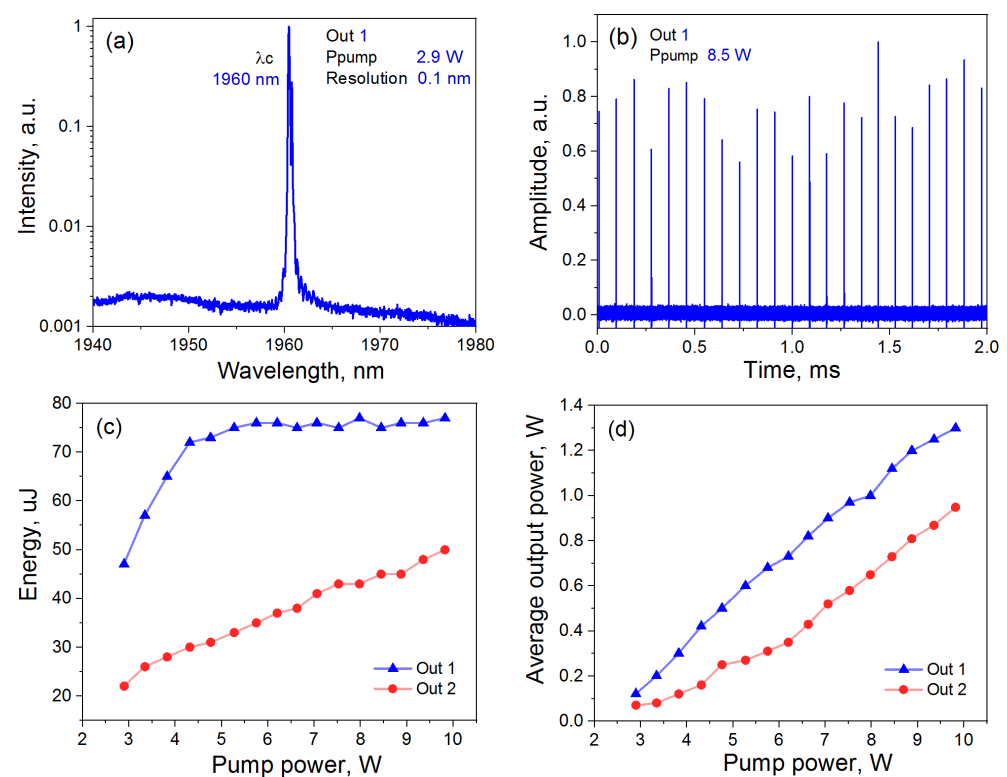


**Figure 2.** (a) Continuous wave radiation spectrum of Tm-doped fiber laser at the output 1; (b) pulse train at a pump power of 8.5 W; (c) pulse energy dependence on the pump power at outputs 1 (blue) and 2 (red); and (d) dependence of average output power on pump power at outputs 1 (blue) and 2 (red).

When the pump power was increased to higher values (2.9–3 W), irregular transitions to pulse generation were observed. In this case, it was not possible to accurately detect the pulse energy and spectra of the output radiation, because the exposure time of the optical spectrum analyzer exceeded the transient time.

To obtain a stable pulse mode, it was necessary to increase the pump power values (more than 3 W). As a result, we observed the continuous pulse train at outputs 1 and 2. The pulse repetition rate increased from 2 to 18 kHz as the pump power increased from 3 to 10 W. Thus, the maximum value of the pulse repetition rate was about 18 kHz and was limited by the pump power. The amplitude fluctuation did not exceed 20%. Figure 2b shows an example of a pulse train with a repetition rate of 11 kHz at a pump power of 8.5 W. Increasing the repetition rate was accompanied by increasing the pulse energy. Figure 2c shows the dependence of energy on pump power at the outputs 1 and 2. The energy of pulses measured at output 1 increased from 47 to 80 μJ, while at output 2, lower energy values were measured from 22 to 50 μJ. From Figure 2c, it is clear that the pulse energy from output 2 increases linearly. We assume that this is caused by the appearance of additional pulses. In contrast, the pulse energy at output 1 saturates at the level of 75–80 μJ. Therefore, we did not observe the appearance of additional pulses, and this may be due to the limited FBG reflection spectrum. Figure 2d shows the dependence of an average output power on the pump power at the laser outputs. The maximum average output power was 1.3 and 0.95 W at outputs 1 and 2, respectively.

The obtained energy values resulted in a nonlinear broadening of the emission spectra up to 450 nm at the level of −20–25 dB directly inside the laser cavity (Figure 3). As can be seen for both outputs, the long wavelength border is limited by the OSA scan range. However, we believe that the spectrum strongly decreases after 2450 nm due to high silica-based fiber losses in this spectral region. Our assumption is confirmed by several investigations [40–42]. In addition, there were side peaks in the spectra (see inset of Figure 3a), related to modulation instability (MI). The maximum frequency offset  $\Omega_{max}$  from the main peak was ~1.2 THz. This corresponds to a peak power of about 3–3.5 kW, if we consider the formula (1) and the cavity fiber data for dispersion ( $\beta_2 = -82 \text{ ps}^2/\text{km}$ ) [43] and nonlinearity ( $\gamma = 0.5 - 1 \text{ W}^{-1} \cdot \text{km}^{-1}$ ).

$$\Omega_{max} = \pm \left( 2\gamma P_0 / |\beta_2| \right)^{1/2}, \tag{1}$$

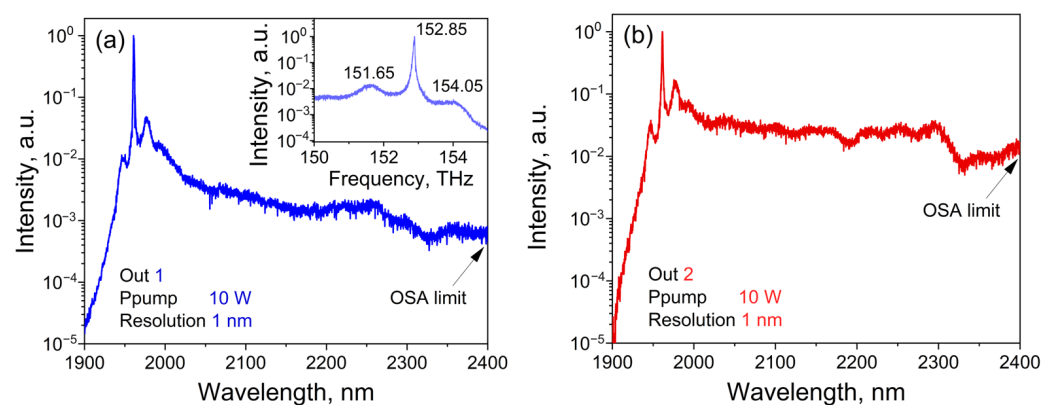


**Figure 3.** Emission spectra at output 1 (a) and 2 (b) of a laser operating in the pulsed mode at a pump power of 10 W. The inset in Figure 3a shows the enlarged side peaks of the spectrum caused by modulation instability.

As known, modulation instability leads to the decay of the initiating pulses into shorter pulses. Thus, the peak power is further increased, which in turn leads to the generation of broadband radiation with an asymmetric spectrum with an extensive flat region in the long-wavelength part, as shown in Figure 3. Such spectra are typical for pumping by single

pulses longer than 1 ps [44] or by pulse bunches [45] into a region of anomalous dispersion far from zero.

Another confirmation of the pulse decay is the observed fine temporal structure of the pulses. The oscilloscope traces at the output of the laser operating in the pulsed mode at a pump power of 10 W are shown in Figure 4a—output 1, and Figure 4b—output 2. Both oscilloscope traces, using the pulse energy data, show values of instantaneous peak pulse power that are significantly higher than those estimated for the MI gain spectrum. However, it is the MI that leads to the formation of bunches of short sub-nanosecond pulses with increased pulse amplitude. That is, it was possible to see the fine structure of the high-energy SBS Q-switched laser pulses. One can note that in this case, the laser is capable of generating bunches of picosecond pulses.

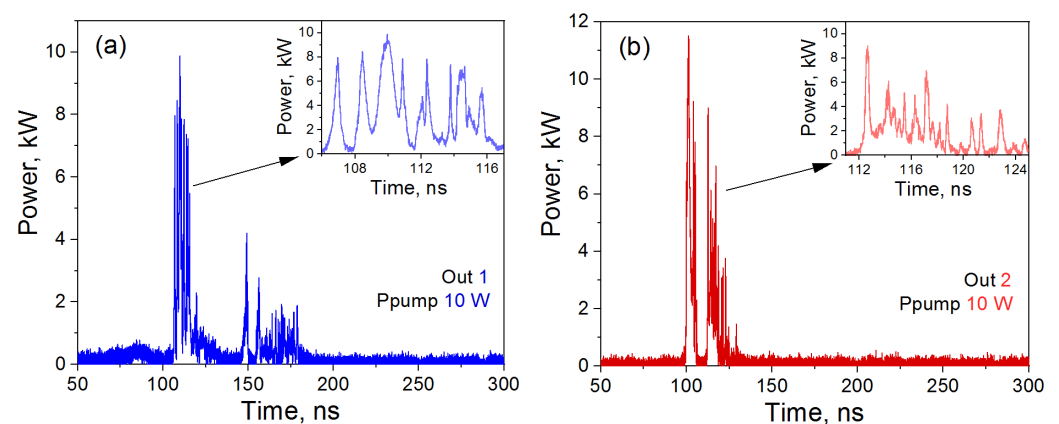


**Figure 4.** Optical pulses at the laser output 1 (a) and 2 (b) at a pump power of 10 W. The insets (a,b) show enlarged areas.

#### 4. Potential Application

We have performed experiments on exposure to radiation from the studied laser on water *in vitro*, and single-spot exposure to collimated pulsed radiation on porcine longissimus muscle tissue *ex vivo*, using the updated setup described in [6]. The choice of this particular biological tissue is determined by its well-known optical properties and high water content [46]. The presence of one of the main water absorption peaks ( $\lambda \approx 1930$  nm) in the 2  $\mu\text{m}$  spectral region makes sources with wavelengths of 1900–2000 nm promising for exposure on water-saturated biological tissues [47]. For *ex vivo* tissue experiments, porcine longissimus muscle tissue was collected after the animal postmortem and pre-cooled to 4 °C. After pre-cooling, the muscle tissue was sliced into small specimens of  $\approx 1$ –3 mm thick. The temperature of the specimens was restored to room temperature (22 °C) prior to the experiments, and the surface of specimens was sprayed with saline to prevent the tissue dehydrating.

Figure 5a shows the schematic of the optical stand for the experiment on non-contact exposure to collimated pulsed radiation of the Tm-doped fiber laser on biological tissue specimens. The pulsed radiation from the first output of the Tm-doped fiber laser (1) was delivered through a single-mode fiber (2) to the optical objective (LOMO). An objective (3) with  $8 \times 0.2$  NA collimated the laser beam positioned normal to the surface of the muscle tissue specimens (4). The loss on the optical objective was about 12%. The laser beam quality was defined by the standard single-mode fiber (core/clad diameter 9/125  $\mu\text{m}$ ) used for the laser radiation output. The diameter of the collimated laser beam with Gaussian intensity distribution on the specimen surface was estimated to be in the range of  $\approx 450$   $\mu\text{m}$ , depending on the objective adjustment and the variation in the specimen thickness. Figure 5b presents a photograph of the result of single-spot exposure to the Tm-doped fiber laser radiation with a pulse repetition rate of 14 kHz, an average power of 1 W, and energy of 72  $\mu\text{J}$  (taking into account objective losses). The exposure time varied between 10 and 20 s. We used a Nikon Eclipse Ci-L 28499 microscope (Nikon, Tokyo, Japan)

at 100× magnification to analyze the specimens' surface after laser radiation exposure, and to obtain photographs.

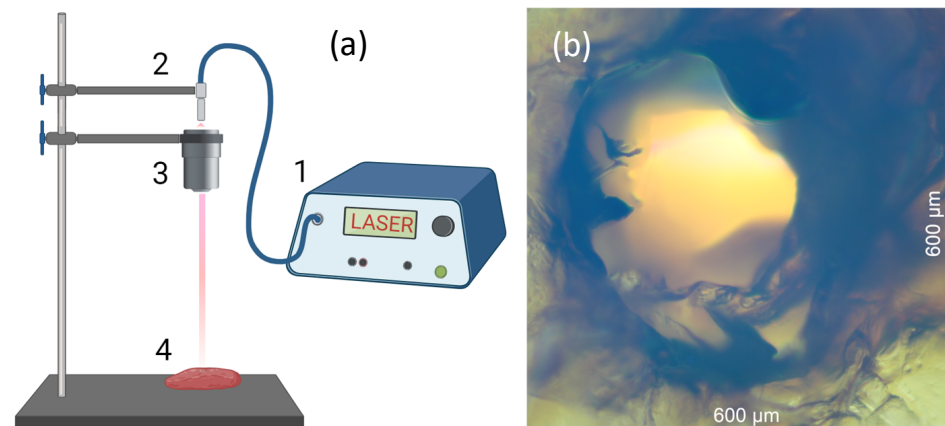


**Figure 5.** (a) The schematic of optical stand for the experiment on non-contact exposure to Tm laser radiation on biological tissue specimens: 1—Tm-doped fiber laser, 2— single-mode fiber for laser radiation delivery, 3— optical objective, 4—muscle tissue specimen; (b) a magnified image of porcine muscle tissue after exposure to pulsed laser radiation with a pulse repetition rate of 14 kHz, an average power of 1, W, and energy of 72  $\mu$ J for 20 s.

According to this photo, it can be seen that exposure to such pulsed radiation leads to the formation of holes in the tissue specimen with a thickness of about 2 mm. The diameter of the holes does not exceed 600  $\mu$ m. In addition, the carbonization of biological tissue is noticeable at the border of the obtained hole. This is due to the high-energy parameters of laser radiation, which lead to a strong overheating of biological tissue and its thermal damage [48]. Thus, it can be concluded that radiation of the developed and studied Tm-doped fiber laser can be used for effective destructive exposure on water-saturated biological tissues. This type of laser radiation, and consequently the compact scheme of an all-fiber laser, may be promising for some medical applications.

## 5. Conclusions

Thus, this paper presents a relatively simple scheme of an all-fiber Tm-doped laser operating in the Q-switching mode due to the SBS effect. The laser scheme consisted of standard commercially available fiber optic components. The fine structure of the obtained pulse radiation with a resolution of 0.1 ns was detected. The supercontinuum spectrum (up to 450 nm) was obtained directly at the laser outputs without using additional fibers with a high nonlinearity coefficient. The pulse energies at the laser outputs were in the range of 22 to 80  $\mu$ J, which allowed the generation of spectrally broadened radiation directly at the laser output. For the first time, the presence of a fine subnanosecond structure in the pulse generation of the SBS laser, obtained due to the effect of modulation instability, has been demonstrated. We have also demonstrated the possibility of using this type of radiation for destructive exposure on soft biological tissues.

**Author Contributions:** Conceptualization, V.A.K., D.A.K., A.A.F. and V.B.T.; methodology, V.A.K., T.I.M. and S.A.F.; investigation, V.A.K., S.A.F., T.I.M. and M.D.C.; resources, V.A.K. and A.A.W.; data curation, V.A.K.; writing—original draft preparation, V.A.K., S.A.F., T.I.M. and D.A.K.; writing—review and editing, A.A.W., A.A.F. and V.B.T.; visualization, V.A.K., S.A.F., T.I.M. and M.D.C.; supervision, V.A.K.; project administration, V.A.K., A.A.F. and V.B.T.; funding acquisition, D.A.K., A.A.F. and V.B.T. All authors have read and agreed to the published version of the manuscript.

**Funding:** This research was supported by the Ministry of Science and Higher Education of the Russian Federation, grant numbers 075-15-2022-315 and 075-15-2021-581, and carried out on the basis of World-Class Research Center Photonics (experiment, data collection, and processing). D.A.K. thanks the Russian Science Foundation, grant number 23-79-30017 (data interpretation). A.A.F. is supported by the European Union's Horizon 2020 research and innovation program (Individual Fellowship, H2020-MSCA-IF-2020, #101028712).

**Institutional Review Board Statement:** Not applicable.

**Informed Consent Statement:** Not applicable.

**Data Availability Statement:** The data supporting the findings of this study are available within the article.

**Conflicts of Interest:** The authors declare no conflicts of interest.

## References

- Zhang, J.; Schulze, F.; Mak, K.F.; Pervak, V.; Bauer, D.; Sutter, D.; Pronin, O. High-Power, High-Efficiency Tm:YAG and Ho:YAG Thin-Disk Lasers. *Laser Photonics Rev.* **2018**, *12*, 1700273. [\[CrossRef\]](#)
- Walsh, B.M. Review of Tm and Ho Materials; Spectroscopy and Lasers. *Laser Phys.* **2009**, *19*, 855–866. [\[CrossRef\]](#)
- Shi, W.; Fang, Q.; Zhu, X.; Norwood, R.A.; Peyghambarian, N. Fiber lasers and their applications. *Appl. Opt.* **2014**, *53*, 6554–6568. [\[CrossRef\]](#) [\[PubMed\]](#)
- Polder, K.D.; Bruce, S. Treatment of Melasma Using a Novel 1,927-nm Fractional Thulium Fiber Laser: A Pilot Study. *Dermatol. Surg.* **2012**, *38*, 199–206. [\[CrossRef\]](#) [\[PubMed\]](#)
- Kopyeva, M.S.; Filatova, S.A.; Kamynin, V.A.; Trikshev, A.I.; Kozlikina, E.I.; Astashov, V.V.; Loschenov, V.B.; Tsvetkov, V.B. Ex Vivo Exposure to Soft Biological Tissues by the 2- $\mu\text{m}$  All-Fiber Ultrafast Holmium Laser System. *Appl. Sci.* **2022**, *12*, 3825. [\[CrossRef\]](#)
- Kopyeva, M.S.; Filatova, S.A.; Kamynin, V.A.; Trikshev, A.I.; Kozlikina, E.I.; Astashov, V.V.; Loschenov, V.B.; Tsvetkov, V.B. Ex-Vivo Exposure on Biological Tissues in the 2- $\mu\text{m}$  Spectral Range with an All-Fiber Continuous-Wave Holmium Laser. *Photonics* **2021**, *9*, 20. [\[CrossRef\]](#)
- Mingareev, I.; Weirauch, F.; Olowinsky, A.; Shah, L.; Kadwani, P.; Richardson, M. Welding of Polymers Using a 2  $\mu\text{m}$  Thulium Fiber Laser. *Opt. Laser Technol.* **2012**, *44*, 2095–2099. [\[CrossRef\]](#)
- Petrovich, M.N.; Poletti, F.; Wooler, J.P.; Heidt, A.M.; Baddela, N.K.; Li, Z.; Gray, D.R.; Slavík, R.; Parmigiani, F.; Wheeler, N.V.; et al. Demonstration of Amplified Data Transmission at 2  $\mu\text{m}$  in a Low-Loss Wide Bandwidth Hollow Core Photonic Bandgap Fiber. *Opt. Express* **2013**, *21*, 28559. [\[CrossRef\]](#)
- Zhang, H.; Kavanagh, N.; Li, Z.; Zhao, J.; Ye, N.; Chen, Y.; Wheeler, N.V.; Wooler, J.P.; Hayes, J.R.; Sandoghchi, S.R.; et al. 100 Gbit/s WDM Transmission at 2  $\mu\text{m}$ : Transmission Studies in Both Low-Loss Hollow Core Photonic Bandgap Fiber and Solid Core Fiber. *Opt. Express* **2015**, *23*, 4946. [\[CrossRef\]](#)
- De Young, R.J.; Barnes, N.P. Profiling Atmospheric Water Vapor Using a Fiber Laser Lidar System. *Appl. Opt.* **2010**, *49*, 562. [\[CrossRef\]](#)
- Spiers, G.D.; Menzies, R.T.; Jacob, J.; Christensen, L.E.; Phillips, M.W.; Choi, Y.; Browell, E.V. Atmospheric CO<sub>2</sub> Measurements with a 2  $\mu\text{m}$  Airborne Laser Absorption Spectrometer Employing Coherent Detection. *Appl. Opt.* **2011**, *50*, 2098. [\[CrossRef\]](#) [\[PubMed\]](#)
- Sennaroglu, A.; Demirbas, U.; Vermeulen, N.; Ottevaere, H.; Thienpont, H. Continuous-Wave Broadly Tunable Cr<sup>2+</sup>:ZnSe Laser Pumped by a Thulium Fiber Laser. *Opt. Commun.* **2006**, *268*, 115–120. [\[CrossRef\]](#)
- Jung, M.; Han Lee, J. Actively Q-Switched, Thulium–Holmium-Codoped Fiber Laser Incorporating a Silicon-Based, Variable-Optical-Attenuator-Based Q Switch. *Appl. Opt.* **2013**, *52*, 2706. [\[CrossRef\]](#) [\[PubMed\]](#)
- Li, F.; Zhu, H.; Zhang, Y. High-Power Widely Tunable Q-Switched Thulium Fiber Lasers. *Laser Phys. Lett.* **2015**, *12*, 095102. [\[CrossRef\]](#)
- Fale, A.E.; Zverev, A.D.; Kamynin, V.A.; Wolf, A.A.; Filatova, S.A.; Nanii, O.E.; Smirnov, A.P.; Fedoseev, A.I.; Tsvetkov, V.B. The Dynamics of Multi-Peak Pulsed Generation in a Q-Switched Thulium-Doped Fiber Laser. *Photonics* **2022**, *9*, 846. [\[CrossRef\]](#)
- Wang, Y.; Xie, G.; Xu, X.; Di, J.; Qin, Z.; Suomalainen, S.; Guina, M.; Härkönen, A.; Agnesi, A.; Griebner, U.; et al. SESAM Mode-Locked Tm:CALGO Laser at 2  $\mu\text{m}$ . *Opt. Mater. Express* **2015**, *6*, 131. [\[CrossRef\]](#)
- Ma, W.; Wang, T.; Su, Q.; Wang, F.; Zhang, J.; Wang, C.; Jiang, H. 1.9  $\mu\text{m}$  Square-Wave Passively Q-Witched Mode-Locked Fiber Laser. *Opt. Express* **2018**, *26*, 12514. [\[CrossRef\]](#)
- Cho, W.B.; Schmidt, A.; Yim, J.H.; Choi, S.Y.; Lee, S.; Rotermund, F.; Griebner, U.; Steinmeyer, G.; Petrov, V.; Mateos, X.; et al. Passive Mode-Locking of a Tm-Doped Bulk Laser near 2  $\mu\text{m}$  Using a Carbon Nanotube Saturable Absorber. *Opt. Express* **2009**, *17*, 11007. [\[CrossRef\]](#)
- Gatti, D.; Galzerano, G.; Toncelli, A.; Tonelli, M.; Laporta, P. Actively Mode-Locked Tm-Ho:LiYF<sub>4</sub> and Tm-Ho:BaY<sub>2</sub>F<sub>8</sub> Lasers. *Appl. Phys. B* **2006**, *86*, 269–273. [\[CrossRef\]](#)
- Tang, Y.; Xu, J. Model and Characteristics of Self-Pulsing in Tm<sup>3+</sup>-Doped Silica Fiber Lasers. *IEEE J. Quantum Electron.* **2011**, *47*, 165–171. [\[CrossRef\]](#)



21. Liu, C.; Luo, Z.; Huang, Y.; Qu, B.; Cheng, H.; Wang, Y.; Wu, D.; Xu, H.; Cai, Z. Self-Mode-Locked 2  $\mu\text{m}$  Tm<sup>3+</sup>-Doped Double-Clad Fiber Laser with a Simple Linear Cavity. *Appl. Opt.* **2014**, *53*, 892. [[CrossRef](#)] [[PubMed](#)]
22. Kirsch, D.C.; Bednyakova, A.; Varak, P.; Honzatko, P.; Cadier, B.; Robin, T.; Fotiadi, A.; Peterka, P.; Chernysheva, M. Gain-Controlled Broadband Tuneability in Self-Mode-Locked Thulium-Doped Fibre Laser. *Commun. Phys.* **2022**, *5*, 219. [[CrossRef](#)]
23. Jiang, M.; Tayebati, P. Stable 10 Ns, Kilowatt Peak-Power Pulse Generation from a Gain-Switched Tm-Doped Fiber Laser. *Opt. Lett.* **2007**, *32*, 1797. [[CrossRef](#)] [[PubMed](#)]
24. Simakov, N.; Hemming, A.; Bennetts, S.; Haub, J. Efficient, Polarised, Gain-Switched Operation of a Tm-Doped Fibre Laser. *Opt. Express* **2011**, *19*, 14949. [[CrossRef](#)] [[PubMed](#)]
25. Koo, J.; Shin, W. Nanosecond Pulse Generation from Actively Q-Switched Thulium-Doped Fiber Laser Using a High-Speed Optical Switch. In *Fiber Lasers XV: Technology and Systems*; SPIE: Bellingham, WA, USA, 2018. [[CrossRef](#)]
26. Coluccelli, N.; Galzerano, G.; Laporta, P.; Parisi, D.; Toncelli, A.; Tonelli, M. Room-Temperature Q-Switched Tm:BaY2F8 Laser Pumped by CW Diode Laser. *Opt. Express* **2006**, *14*, 1518. [[CrossRef](#)] [[PubMed](#)]
27. Sadovnikova, Y.E.; Kamynin, V.A.; Kurkov, A.S.; Medvedkov, O.I.; Marakulin, A.V.; Minashina, L.A. Q-Switching of a Thulium-Doped Fibre Laser Using a Holmium-Doped Fibre Saturable Absorber. *Quantum Electron.* **2014**, *44*, 4–6. [[CrossRef](#)]
28. Zverev, A.D.; Kamynin, V.A.; Trikshev, A.I.; Kovtun, E.Y.; Arutyunyan, N.R.; Mastin, A.A.; Ryabochkina, P.A.; Obratsova, E.D.; Tsvetkov, V.B. Influence of Saturable Absorber Parameters on the Operation Regimes of a Dumbbell-Shaped Thulium Fibre Laser. *Quantum Electron.* **2021**, *51*, 518–524. [[CrossRef](#)]
29. Luo, Z.; Liu, C.; Huang, Y.; Wu, D.; Wu, J.; Xu, H.; Cai, Z.; Lin, Z.; Sun, L.; Weng, J. Topological-Insulator Passively Q-Switched Double-Clad Fiber Laser at 2  $\mu\text{m}$  Wavelength. *IEEE J. Select. Top. Quantum Electron.* **2014**, *20*, 0902708. [[CrossRef](#)]
30. Chernikov, S.V.; Zhu, Y.; Taylor, J.R.; Gapontsev, V.P. Supercontinuum Self-Q-Switched Ytterbium Fiber Laser. *Opt. Lett.* **1997**, *22*, 298. [[CrossRef](#)]
31. Fotiadi, A.A.; Mégret, P.; Blondel, M. Dynamics of a Self-Q-Switched Fiber Laser with a Rayleigh–Stimulated Brillouin Scattering Ring Mirror. *Opt. Lett.* **2004**, *29*, 1078. [[CrossRef](#)]
32. Gruk, D.A.; Kurkov, A.S.; Razdobreev, I.M.; Fotiadi, A.A. Self-Q-Switched Ytterbium-Doped Cladding-Pumped Fibre Laser. *Quantum Electron.* **2002**, *32*, 1017–1019. [[CrossRef](#)]
33. Hou, S.; Lou, Y.; Zhao, N.; Chen, P.; Zhang, F.; Chen, Y.; Lin, F.; Li, J.; Yang, L.; Peng, J.; et al. Robust Q-Switching Based on Stimulated Brillouin Scattering Assisted by Fabry-Perot Interference. *Opt. Express* **2019**, *27*, 5745. [[CrossRef](#)] [[PubMed](#)]
34. Tang, Y.; Li, X.; Wang, Q.J. High-Power Passively Q-Switched Thulium Fiber Laser with Distributed Stimulated Brillouin Scattering. *Opt. Lett.* **2013**, *38*, 5474. [[CrossRef](#)] [[PubMed](#)]
35. Fotiadi, A.A.; Mégret, P. Self-Q-Switched Er-Brillouin Fiber Source with Extra-Cavity Generation of a Raman Supercontinuum in a Dispersion-Shifted Fiber. *Opt. Lett.* **2006**, *31*, 1621. [[CrossRef](#)] [[PubMed](#)]
36. Dostovalov, A.V.; Wolf, A.A.; Parygin, A.V.; Zyubin, V.E.; Babin, S.A. Femtosecond Point-by-Point Inscription of Bragg Gratings by Drawing a Coated Fiber through Ferrule. *Opt. Express* **2016**, *24*, 16232. [[CrossRef](#)] [[PubMed](#)]
37. Fotiadi, A.A. An Incoherent Fibre Laser. *Nat. Photon* **2010**, *4*, 204–205. [[CrossRef](#)]
38. Fotiadi, A.A.; Kiyani, R.; Deparis, O.; Mégret, P.; Blondel, M. Statistical Properties of Stimulated Brillouin Scattering in Single-Mode Optical Fibers above Threshold. *Opt. Lett.* **2002**, *27*, 83. [[CrossRef](#)]
39. Turitsyn, S.K.; Babin, S.A.; El-Taher, A.E.; Harper, P.; Churkin, D.V.; Kablukov, S.I.; Ania-Castañón, J.D.; Karalekas, V.; Podivilov, E.V. Random Distributed Feedback Fibre Laser. *Nat. Photon* **2010**, *4*, 231–235. [[CrossRef](#)]
40. Dvoyrin, V.V.; Sorokina, I.T. 6.8 W All-Fiber Supercontinuum Source at 1.9–2.5  $\mu\text{m}$ . *Laser Phys. Lett.* **2014**, *11*, 085108. [[CrossRef](#)]
41. Tao, M.; Yu, T.; Wang, Z.; Chen, H.; Shen, Y.; Feng, G.; Ye, X. Super-Flat Supercontinuum Generation from a Tm-Doped Fiber Amplifier. *Sci. Rep.* **2016**, *6*, 23759. [[CrossRef](#)]
42. Heidt, A.M.; Modupeh Hodasi, J.; Rampur, A.; Spangenberg, D.-M.; Ryser, M.; Klimczak, M.; Feurer, T. Low Noise All-Fiber Amplification of a Coherent Supercontinuum at 2  $\mu\text{m}$  and Its Limits Imposed by Polarization Noise. *Sci. Rep.* **2020**, *10*, 16734. [[CrossRef](#)] [[PubMed](#)]
43. Ciacka, P.; Rampur, A.; Heidt, A.; Feurer, T.; Klimczak, M. Dispersion Measurement of Ultra-High Numerical Aperture Fibers Covering Thulium, Holmium, and Erbium Emission Wavelengths. *J. Opt. Soc. Am. B* **2018**, *35*, 1301. [[CrossRef](#)]
44. Kamynin, V.A.; Kurkov, A.S.; Mashinsky, V.M. Supercontinuum Generation up to 2.7  $\mu\text{m}$  in the Germanate-Glass-Core and Silica-Glass-Cladding Fiber. *Laser Phys. Lett.* **2012**, *9*, 219–222. [[CrossRef](#)]
45. Klimentov, D.; Tolstik, N.; Dvoyrin, V.V.; Richter, R.; Sorokina, I.T. Flat-Top Supercontinuum and Tunable Femtosecond Fiber Laser Sources at 1.9–2.5  $\mu\text{m}$ . *J. Light. Technol.* **2016**, *34*, 4847–4855. [[CrossRef](#)]
46. Bashkatov, A.N.; Genina, E.A.; Tuchin, V.V. Optical Properties of Skin, Subcutaneous, and Muscle Tissues: A Review. *J. Innov. Opt. Health Sci.* **2011**, *4*, 9–38. [[CrossRef](#)]
47. Filatova, S.A.; Shcherbakov, I.A.; Tsvetkov, V.B. Optical Properties of Animal Tissues in the Wavelength Range from 350 to 2600 nm. *J. Biomed. Opt.* **2017**, *22*, 035009. [[CrossRef](#)]
48. Niemz, M.H. *Laser-Tissue Interactions*; Springer: Berlin/Heidelberg, Germany, 2007.

**Disclaimer/Publisher’s Note:** The statements, opinions and data contained in all publications are solely those of the individual author(s) and contributor(s) and not of MDPI and/or the editor(s). MDPI and/or the editor(s) disclaim responsibility for any injury to people or property resulting from any ideas, methods, instructions or products referred to in the content.